Computer Methods and Programs in Biomedicine 261 (2025) 108591

Contents lists available at ScienceDirect

Computer Methods and Programs in Biomedicine

journal homepage: www.sciencedirect.com/journal/computer-methods-and-programs-in-biomedicine

# Automatic path planning for pelvic fracture reduction with multi-degree-of-freedom

Chao Shi [a], Qing Yang [b], Yuantian Wang [a], Xiangrui Zhao [c], Shuchang Shi [c], Lijia Zhang [c], Sutuke Yibulayimu [a], Yanzhen Liu [a], Chendi Liang [a], Yu Wang [a,*], Chunpeng Zhao [d]

[a] Key Laboratory of Biomechanics and Mechanobiology (Beihang University), Ministry of Education, Beijing Advanced Innovation Center for Biomedical Engineering, School of Biological Science and Medical Engineering, Beihang University, Beijing, 100083, China
[b] Qingdao Hospital, University of Health and Rehabilitation Sciences (Qingdao Municipal Hospital), Qingdao, China
[c] Rossum Robot Co., Ltd, Beijing, China
[d] Department of Orthopaedics and Traumatology, Beijing Jishuitan Hospital, Beijing, China

ARTICLE INFO

*Keywords:*
Computer-assisted surgery
Pelvic fracture
Fracture reduction
Path planning
Collision detection

ABSTRACT

*Background and objectives:* Computer-assisted orthopedic surgical techniques and robotics has improved the therapeutic outcome of pelvic fracture reduction surgery. The preoperative reduction path is one of the prerequisites for robotic movement and an essential reference for manual operation. As the largest irregular bone with complicated morphology, the rotational motion of pelvic fracture fragments impacts the reduction process directly. To address this, the primary objective of this study is to develop an efficient and effective algorithm for automatically planning the reduction trajectory in robot-assisted pelvic fracture surgeries.
*Methods:* After obtaining rotational and reorientated translational degrees of freedom through the initial and target positions of the fracture fragments, the initial path is acquired through improved path planning method combined with specific designed collision detection algorithm. The final reduction path is post-processed to be shortened and smoothed. The effectiveness of the algorithm was evaluated in various pelvic fracture models with surrounding muscles and was compared with prior relevant implementations.
*Results:* Simulation results showed the ability of the planner to save time and overcome the state of art in terms of collision detection, path length and smoothness, search time, and surrounding muscle stretching conditions.
*Conclusions:* The proposed method enables a reasonable reduction path for pelvic fracture, which is demonstrated to be superior in various pelvic fracture scenarios.

## 1. Introduction

Accounting for 2–8 % of all fractures, pelvic fracture is a serious, high-energy injury with a disability rate of about 60 % and a mortality rate of >13 % [1–3], both of which are the highest of all types of fractures. Pelvic ring disruption and fracture displacement are two main characters of pelvic fracture. Therefore, the first and most important step in surgical treatment is fracture reduction [4].As the intermediate connection of the body, poor pelvic fracture reduction may lead to deformed healing, unequal leg lengths, and secondary lumbar spine, hip, and knee dysfunction, which could seriously affect the patient's life. According to long-term clinical follow-ups with large samples, persistent pain happened in 63 % of the patients [5], 28 % had sensory and motor abnormalities [6], and 32 % couldn't continue their previous job [7].

In conventional surgery, open procedure is performed to expose and visualize the fracture, followed by empirically planning and manual reduction. However, due to the complexity of pelvic fractures and the limited precision of manual manipulation, this approach is often associated with a higher risk of infection and soft tissue failure, leading to prolonged hospitalization, rehabilitation time, substantial costs, together with empirically determined surgical outcomes [8,9]. Computer-assisted surgical techniques have been developed to alleviate these problems. Various (semi-)automatic deep learning-based segmentation methods have recently been proposed to create three-dimensional (3D) models of bone fragments that accurately represent the bones and fragments affected by injury [10–13]. Fracture line matching, contralateral mirroring template and statistical shape models (SSMs) provide effective reference for planning target position

* Corresponding author.
*E-mail address:* wangyu@buaa.edu.cn (Y. Wang).

https://doi.org/10.1016/j.cmpb.2025.108591
Received 4 September 2024; Received in revised form 29 December 2024; Accepted 5 January 2025
Available online 6 January 2025
0169-2607/© 2025 Published by Elsevier B.V.

for fracture fragments [14–17]. Surgical navigation systems and robots enable stable and accurate operations in closed fracture reduction surgery [17–20]. The above researches have focused on navigational localization and pelvic reconstruction to obtain the target position. However, the target position could not provide a concrete moving programme for the surgery. Rational preoperative planning is crucial in pelvic fracture reduction surgery to design optimal surgical paths and plans, enhancing the procedure's safety and success rate. A reasonable reduction path can reduce intraoperative injuries, making it a prerequisite for automatic and safe operation of the robot and an important reference for manual reduction.

Anatomical knowledge-based manual planning is the simplest and commonly used method, with the reduction path being planned by the surgeon preoperatively, and then executed and adjusted intraoperatively. Dagnino et al. manually planned desired paths for their robot-assisted joint fracture reduction robot [9,21–23]. However, this approach is time-consuming and heavily reliant on the personal skills and experience of the surgeon. Therefore, scholars have classified and quantified the planned path to obtain rules free from subjective experience. Westphal et al. developed a cost function that considered both the amount of distraction and rotation to determine the optimal direction to the fracture region consistent with the soft tissue constraints [24,25]. Du et al. defined a new long bone diaphysis fracture classification based on the application of computer-assisted orthopaedic surgery, and proposed a corresponding reduction path planning strategy based on different fracture types [26]. Subsequently, they proposed a preoperative planning criterion based on the shortest straight-line distance and safety, which contains three basic guidelines for reduction [27]. Based on these strategies, some simple path planning methods were devised. Ruihua Ye et al. designed an algorithm based on the shortest linear path for long bone simple fractures [28], where the reduction bone is rotated around the medial axis, and adjusted in real time during the operation to finally reach the target position. Kim et al. used a linear guidance constraint (LGC) controller to guide the distal fracture segment by uniformly reducing translational and rotational misalignment, while the surgeon can manually modify the path at any time [19]. In our previous work, similar algorithm was devised for the generation of shortest reduction path [29]. One or several transition waypoints were set manually to avoid collision. The fractured bone moved to the waypoint in sequence and eventually came to the target position.

The above manual and semi-automatic methods could help surgeons to plan safe reduction path that meet the clinical requirements. However, due to the subjectivity of surgeons, the planned path can barely be guaranteed to be optimal with the shortest moving distance and the least impact on the surrounding soft tissues. In addition, these methods are time-consuming.

Automatic path planning methods provide rational path from the current location to the target location within the working environment based on one (or several) predefined criteria. Nowadays, these methods are fruitfully employed in many fields, such as transportation, entertainment, mining, rescuing, education, military, space, agriculture etc. Commonly used path planning methods include artificial potential field method, graph-based method, sampling-based method, learning-based method and bionic method [30–34]. Among them, graph-search methods are based on the discrete approximation of the planning problem. They are "resolution complete" as they can determine in a finite time whether a solution exists, and "resolution optimal" as they can estimate the best path given a specific resolution. With these characteristics, graph-based methods have been widely used in fracture reduction path planning over the last few years. Buschbaum et al. proposed an automatic path planning method for femur fracture reduction based on previous work of fracture line matching [15], where muscle forces during reduction are considered through musculoskeletal simulation models and the A* algorithm is used for reduction path planning after orientation adjusted. Similarly, Xu et al. utilized intersection test of real-time updated point cloud to detect collision, and incorporated muscle length constraints into the improved A* path planning method for femur fracture reduction after achieving rotational alignment, avoiding overstretching of the surrounding muscles during reduction [35]. Pan et al. proposed an improved 3D-OPS A* algorithm by combing orientation planning strategy (OPS) and liner sampling search (LSS) into A* algorithm, with rotation uniformly distributed along Z-axis during path search, and collision detection through octree combined with AABB bounding box [36]. Further, an OpenSim-based pelvic fracture reduction model was constructed, and real-time reduction force based on this model was calculated and incorporated into path planning to obtain better path with less overall reduction force [37].

Notably, above methods take only three degree-of-freedom (DOF) movements into account for planning, and mostly adopt the reduction strategy of first traction then rotation and finally translation. The rotation and translation in the reduction process are split during operation, with the rotation aligned manually first, followed by improved A* method in the translation phase. This strategy is applicable for long bone fractures, which are regular in shape and have a large peripheral buffer space available for adjustment, but for the pelvis, where complex fractures are more difficult to reduce, translations followed by rotations may lead to large path redundancy. Binding the rotation with a certain translation direction to reduce the planning DOFs makes it difficult to obtain a feasible solution for such complex fractures. Meanwhile, the relative simpleness of these methodologies conflicts with the high computation time necessary to solve the optimal planning problem in high dimensional cases, as the discretization of the environment becomes finer (so-called curse of dimensionality [38,39]). This has been mentioned in some previous researches [35–37]. Meanwhile, collision detection methods based on intersection test or the combination of Octree and AABB bounding box cannot satisfy the efficiency and high accuracy needs of surgical procedures.

To address this, the current study presents a new path planning algorithm capable of implementation on different pelvic fracture reduction scenarios. This work attempts to fulfill the following criteria: (1) fast and precise collision detection; (2) multi-DOF planning considering rotations; (3) balance between computational efficiency and moving distance; (4) less impact on surrounding tissues; (5) possibility of generating automatically.

## 2. Method

### 2.1. Overview

Fig. 1 depicts the main components of the proposed path planning method. The input consists of 3D reconstructed models of pelvic fracture fragments obtained by segmentation and target position for reduction based on our previous works [13,14]. The algorithm is comprised of four methodologies:

a) Acquisition of search degree-of-freedom
The dimensionality and direction for path search are required prior to planning. Rotation is incorporated as a separate DOF in the path search in addition to 3 DOFs of translation, which is obtained by the initial and target positions of fracture reduction. The translational DOFs are also optimized for redirection to keep the movement evenly distributed in each direction.
b) Fast and precise collision detection
The collision detection method consists of two main parts, bounding spheres formation and two-level collision detection. Compact personalized hierarchies of fracture fragments were generated firstly, with real-time updating of their positions during planning. Then triangular facets with collision potential through interaction between hierarchies and accurate results are obtained by means of precise detection.
c) Improved lazy A* path planning
To combat the curse of dimensionality, the conventional A*

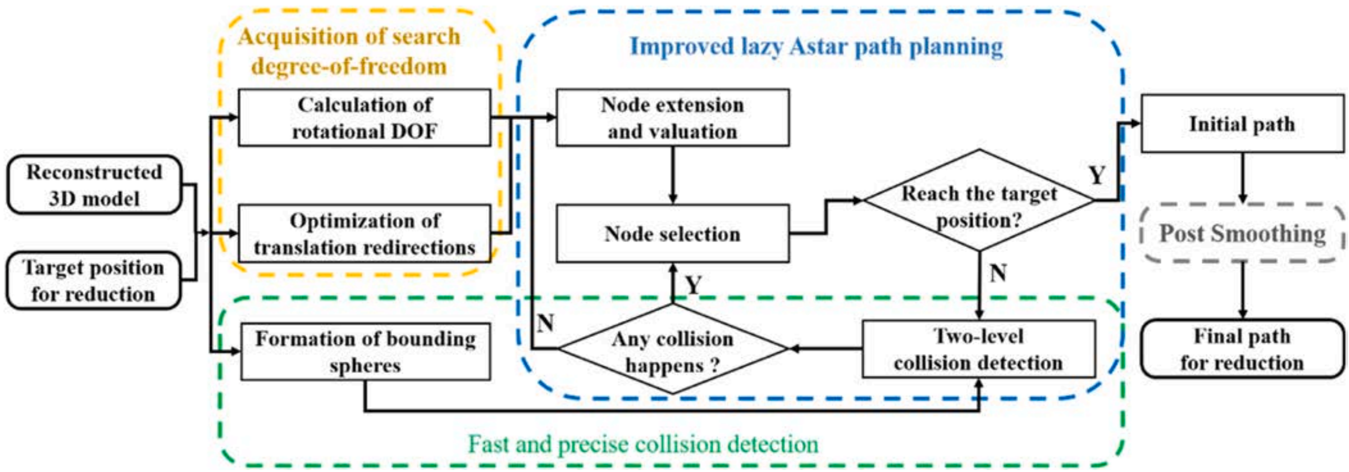


**Fig. 1.** Overview of the proposed algorithm.

method is optimized to improve its computational efficiency by two aspects: (1) Postponing the collision detection part to reduce the number of collision tests. (2) Adjusting the computation of the heuristic function to improve its goal convergence.

d) Post smoothing

For the problem of path redundancy, the initial path previously acquired is post-processed to be shortened and smoothed with the 3D model-based line-of-sight (LOS) algorithm. The desired reduction path is finally obtained.

### 2.2. Acquisition of search degree-of-freedom

#### 2.2.1. Definition of rotational degree-of-freedom

Existing path planning methods generally focus on 3D spatial position of objects, and some flexible machines and vehicles also need to consider the kinematic accessibility of the path [30–32]. Nevertheless, pelvic fracture reduction is rather different, as poor rotational reduction of fracture fragments could have direct impact on surgical outcome. Therefore, it could be regarded as a proximity splicing task of objects in complex in vivo environment, where both translation and rotation of the fracture fragment should be considered. In this study, rotation is incorporated as a separate DOF in the path search. The initial and target positions of the fracture fragment are represented as

$$\begin{cases} S_{start} = \left[x_{start},\ y_{start},\ z_{start},\ \vec{0}\right] \\ S_{goal} = \left[x_{goal},\ y_{goal},\ z_{goal},\ \overrightarrow{\boldsymbol{RV}}\right] \end{cases} \tag{1}$$

Where $S_{start}$ is the initial state of the path planning, including translation parameters $[x_{start}, y_{start}, z_{start}]$ and rotation parameters $\vec{0}$ two parts. $S_{goal}$ is the target state of the path planning, contains the same parameters as above. $[x_{start}, y_{start}, z_{start}]$ and $[x_{goal}, y_{goal}, z_{goal}]$ are the centroid of each point cloud. Since rotational vector is adopted as rotational DOF in this study, $\vec{0}$ is the rotation parameter of the initial state, and $\overrightarrow{\boldsymbol{RV}}$ is the rotation vector (the product of the unit vector and the angle of rotation) transformed by the rotation matrix between the initial state and the target state. The subsequent search node representations are the same as in Eq. (1). These parameters could be transformed into the rotation matrix, and followed by the point cloud data of this node. In this study, the 3D principal axes of the point cloud of the initial state and the target state are obtained separately by principal component analysis (PCA) to get the rotation matrix between them, and finally $\overrightarrow{\boldsymbol{RV}}$. It could also be obtained through registration method. Based on the above state parameters, the search direction in this study contains four DOFs, namely translation in three directions and rotation around the rotation vector.

#### 2.2.2. Redirection optimization of translational search

Notably, the fixed search step size for heuristic search may lead to mismatched resolution since the moving distance varied greatly among different pelvic fractures. Therefore, the line from $[x_{start}, y_{start}, z_{start}]$ to $[x_{goal}, y_{goal}, z_{goal}]$ is used as a diagonal line, and the displacements in the three directions corresponding to the diagonal line are segmented by a fixed number of steps $NS$ instead of a fixed search step length, enabling adaptive adjustment of the search resolution. However, direct translation on the original xyz-axis can result in significant differences in moving distance on different axes, as shown in the blue grid on Fig. 2(a). Since discrete collision detection method is adopted in this study, where one new position is subjected to one collision detection, to avoid overcrowded search in the direction of small moving steps and reduce the tunneling effect in the direction of large steps, homogenous distribution of the moving length in each direction is required. The green grid in Fig. 2(a) shows the optimized solution, capable of a larger search space than the blue grid with the same number of search nodes.

Low DOFs in the 2D plane make it feasible for translational optimization, whereas redundant degree of freedom exists in 3D space, where the three directions perpendicular to each other are capable of rotating around the diagonal. Based on the ring-shaped characteristics of the pelvis, a geometric approach was devised, shown in Fig. 2(c). Firstly, the centroid of the whole pelvis after reduction is calculated through the reduction target position and the main pelvic fragment, which is *Center* in Fig. 2. One of the translational directions $\vec{l_1}$ is then set to be in the plane of *Center, Start* and *Goal.* The other two translational directions $\vec{l_2}$ and $\vec{l_3}$ can also be determined after $\vec{l_1}$. The calculation of translational parameters is shown below.

$$\begin{cases} \vec{l_1} = \sqrt{\dfrac{1}{3}}\left(\dfrac{\overrightarrow{V_{GS}}}{\left|\overrightarrow{V_{GS}}\right|}\right) + \sqrt{\dfrac{2}{3}}\left(\dfrac{\overrightarrow{V_C}}{\left|\overrightarrow{V_C}\right|}\right) \\ \vec{l_2} = \left(\sqrt{3}\left(\dfrac{\overrightarrow{V_{GS}}}{\left|\overrightarrow{V_{GS}}\right|}\right) - \vec{l_1}\right) \times \vec{l_1} \\ \vec{l_3} = \vec{l_1} \times \vec{l_2} \\ d_T = \dfrac{\left|\left[x_{start},\ y_{start},\ z_{start}\right] - \left[x_{goal},\ y_{goal},\ z_{goal}\right]\right|}{\sqrt{3}NS} \end{cases} \tag{2}$$

Where $\overrightarrow{V_C}$ is the perpendicular vector from *Center* to the line on which *Start* and *Goal* are located, and $\overrightarrow{V_{GS}}$ is the direction vector from *Start* to *Goal.* $d_T$ is the translational step distance in each direction.

With the translational step obtained, the point cloud rotational displacement with the centroid of broken bone as the rotation centre

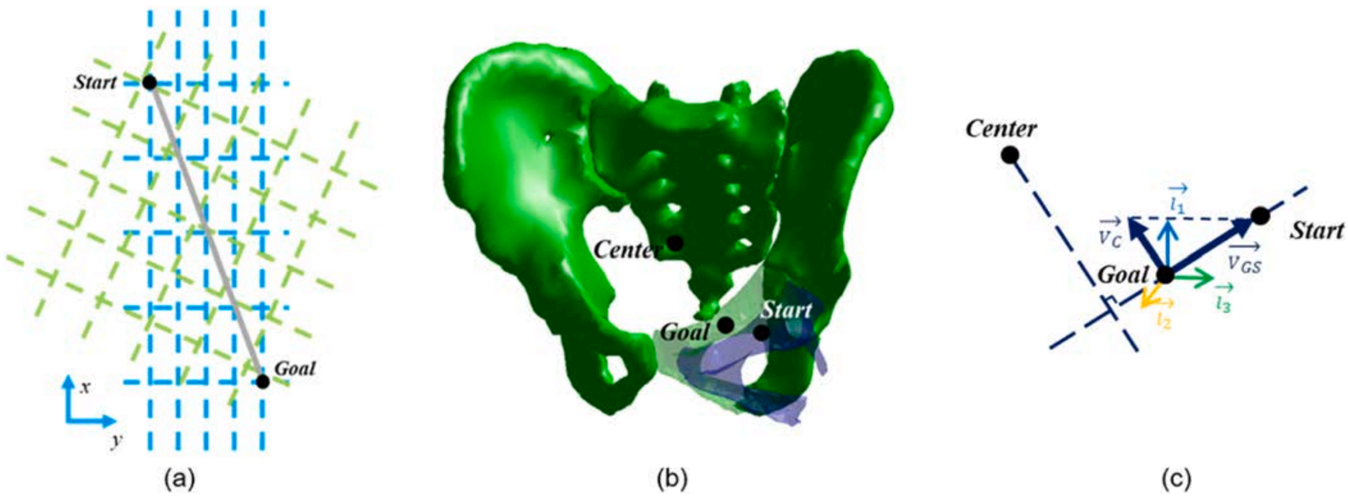


**Fig. 2.** Redirection optimization of translational search. (a) Search based on the original axes (blue grid) and optimized axes (green grid), with the optimized search moving uniformly in all directions; (b) Pelvic fracture model, Center is the centroid of the whole pelvis after reduction, *Start* and *Goal* are the centroids of the fracture fragment at the initial and target position respectively; (c) The optimized directions are obtained by firstly getting $\overrightarrow{l_1}$ through $\overrightarrow{V_C}$ and $\overrightarrow{V_{GS}}$, then $\overrightarrow{l_2}$ and $\overrightarrow{l_3}$.

(from the pose of initial state to target state) is calculated and divided by $d_T$ to obtain the number of rotational steps, and finally the angle of rotational step $\overrightarrow{\boldsymbol{rv}}$. The approximation of the translational and rotational displacements in moving distance is guaranteed for each step.

$$\overrightarrow{\boldsymbol{rv}} = \frac{\overrightarrow{\boldsymbol{RV}}}{round\left(\frac{\sum_{i=1}^{num}\left|{}^{Goal}_{Start}\boldsymbol{R}\cdot[x_i,\ y_i,\ z_i]' - [x_i,\ y_i,\ z_i]'\right|}{num\times d_T}\right)} \quad (3)$$

Where ${}^{Goal}_{Start}\boldsymbol{R}$ is a $3 \times 3$ rotation matrix converted from $\overrightarrow{\boldsymbol{RV}}$. $[x_i, y_i, z_i]$ is the point of the fracture fragment point cloud at initial state. *num* is the number of points in the point cloud.

### 2.3. Fast and precise collision detection

Collision detection between bone fragments is inevitable during planning. The conventional AABB Octree method (Octree combined with AABB bounding box) was frequently applied in computer-aided surgery [36,37,40–42], with its simple and rapid construction of hierarchical tree and collision detection. Nonetheless, AABB Octree method

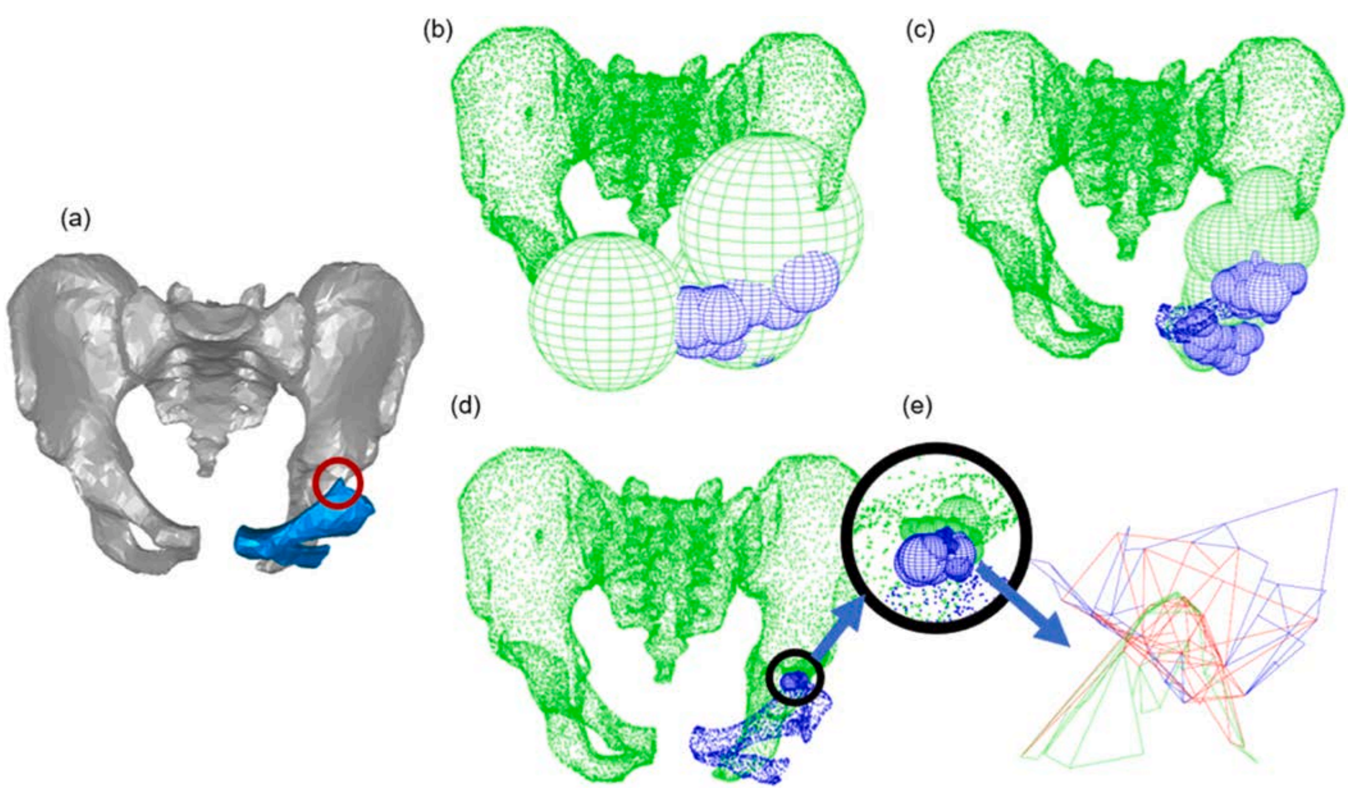


**Fig. 3.** Two level collision detection based on bounding sphere hierarchy. (a) Pelvic fracture model with collision overlaps between bone fragments, read region is where collision occurs. (b)~(d) are the fast detection phase, with overlap between bounding spheres of two hierarchies is checked layer-by-layer, up to the basic spheres. (e) is the precise detection phase, where intersection of their corresponding triangular facets is examined.

requires reasonable size of minimum bounding boxes, with undersize may result in voids leading to discontinuities in the model, and oversize can lead to large errors. Above problems are unacceptable for high-precision surgical procedures. To address this, a fast and precise collision detection method for detailed and complex physiological structures is applied to path planning, which is comprised of bounding spheres formation and two-level collision detection two parts.

The bounding sphere hierarchies of candidate models are created prior to collision detection, according to following steps: (1) Circumspheres are used as the bounding units for basic triangular surfaces, and a specific surface subdivision method is devised to provide better tight wrapping of the model. (2) Hierarchy of bounding spheres established by improved Bi K-means clustering method, with detailed adjustments implemented.

The real-time position and orientation of models are obtained from during planning, allowing the constructed hierarchy to be exploited. Shown in Fig. 3, two-level collision detection is implemented for enhanced efficiency: (1) Fast detection phase, the overlap condition between bounding spheres of two hierarchies is checked layer-by-layer, up to the basic spheres. (2) Precise detection phase, for overlapping basic spheres, the intersection of their corresponding triangular facets is further examined. With the above steps, the detection is capable of rapidly reaching the basic triangular facets of fracture fragments, thus enabling fast and accurate collision detection. More technical details are described in [43], which has been proven to outperform the commonly used AABB Octree method.

### 2.4. Improved Lazy A* path planning

#### 2.4.1. Traditional A* method

As a classical path planning method, A* algorithm combines the advantages of the Dijkstra and BFS (Breadth-First-Search) algorithms and is capable of finding the minimum estimation path in a static search grid through heuristic function. Path with the smallest valuation could always be obtained by A* algorithm in case of paths existing in the search grid [33]. The standard heuristic function is:

$$f(n) = g(n) + h(n) \tag{4}$$

Where $f$(n) is a heuristic function consisting of the actual moving cost $g$(n) for that node to the initial position and the estimated moving cost $h$(n) for that node to the target position. The moving cost is normally computed in terms of Manhattan distance or Euclidean distance, the latter being used in this study.

#### 2.4.2. Improved method

The traditional A* algorithm is simple with the advantages of "resolution complete" and "resolution optimal". To reduce the impact of the "curse of dimensionality", the workflow of the algorithm and the heuristic function are adjusted in this research. The function of various lists available to the method is shown in Table 2. Specific steps are described as follow.

**Step 1**: Initialization. Adding the initial state and its heuristic function value ($f(n)$) to the Open List and g List to initialize each list, where the actual moving cost of the initial state g = 0. To reduce computational effort, the search is performed in the inverse way, taking the target position of fracture reduction as the initial state of the search.

**Step 2**: Select the node to be extended. The node with smallest $f(n)$ is selected from the Open List, and detected whether it has reached the target state. If so, jump to Step 6. If not, continue to Step 3.

**Step 3**: Collision detection. Find the detection result of this node in the Collision List, if no result is detected, then perform the collision detection method in Section 2.3 and add the detection result to the Collision List. Remove this node from the Open list and add it to the Close list.

**Step 4**: Expand the node and calculate the moving cost of child nodes: If no collision occurs at this node, expand it with four search DOFs from Section 2.2 to obtain $3^4-1 = 80$ extended nodes, and assign the $f(n)$ of each child node by Eq. (5) and add it to the Open List.

$$f(n) = g(n) + w * h(n) \tag{5}$$

Eq. (5) adjusts the weight of $g$(n) and $h$(n) in $f$(n). When $w > 1$, the algorithm converges to the BFS method, which is more goal-directed and improves the overall computational efficiency, but also reduces the constraint of the path length, which makes the generated path longer. The change is more obvious with larger $w$. Integrating computational effort and path length, $w$=1.5 in this research.

$g$(n) of the child node is the $g$(n) of expanded parent node plus the moving distance from parent node to the child node. Due to the inclusion of rotational DOF, the above moving distance are calculated as the average moving distance of all points on the model point cloud. Taking $h$(n) as an example:

$$h(n) = \frac{\sum_{i=1}^{num} \left| [x_i, y_i, z_i] - \left[x_{goal\_i},\ y_{goal\_i}, z_{goal\_i}\right] \right|}{num} \tag{6}$$

Where $[x_i, y_i, z_i]$ is the point of fracture fragment point cloud of the node, and $\left[x_{goal\_i}, y_{goal\_i}, z_{goal\_i}\right]$ is the point on the reduction target state point cloud corresponding to $[x_i, y_i, z_i]$.

If the node collides, back to Step 2.

**Step 5**: Update each list. Search the extended child node in the g List, if the node does not exist or the g value calculated in Step 4 is less than that in the g List, then update the g List and the Parent-child List. The decision to update the Open List is then determined in the same way through comparison of the f-values. Then back to Step 2.

**Step 6**: Obtain the initial path. Once the search reaches the target state, the path is backtracked through the Parent-child List. Through iteratively finding the parent node, the path from the target state to the initial state is finally obtained, which is the optimal moving path based on the $f$(n).

### 2.5. Post smoothing

With the adjustment of the heuristic function for efficiency, the generated path may be redundant. Meanwhile, due to the uniform discretization of the space, the generated initial path is fixed by the shape of the mesh, as shown by the red path in Fig. 4. With many unnecessary turns, the blue path is not the optimal path. Therefore, the line-of-sight algorithm (LOS) is employed to optimize the initial path. The nodes on initial path $[S_0, S_1, S_2, \cdots, S_{end}]$, where $S_0 = S_{start}$ and $S_{end} = S_{goal}$. Firstly, taking $S_0$ as one end to connect with its farthest end $S_{end}$ and interpolating uniformly on the connecting line (yellow stars in Fig. 4), where collision detection is performed on these intermediate states. If all these states are collision-free, the direct movement from $S_0$ to $S_{end}$ without any collision is feasible, and the path could be shortened through removing the interval nodes $[S_1, S_2, S_3, \cdots, S_{end-1}]$. If any collision happens, the other end is pushed forward to detect possible direct movement between $S_0$ and $S_{end-1}$. Repeat the above reachability test, and push the node backward after ending $S_0$ until the whole path has been post smoothed. The post-processed path is shown as the blue path in Fig. 4. The optimal reduction path is finally obtained.

**Table 1**
Implication of each list.

| Notification | Implication |
|---|---|
| Open List | Node-set to be extended, including translational and rotational parameters and their evaluations |
| Close List | Extended node-set, with the same content as above |
| Collision List | Collision detection results of nodes |
| g List | The actual moving cost of nodes (from initial position) |
| Parent-child List | Node-set preserving parent-child correspondences |

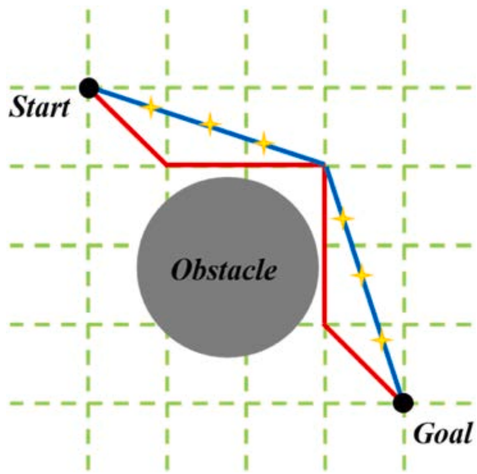


**Fig. 4.** Post smoothing process. The red path is the initial path generated by A* algorithm. The blue path is the path after post smoothing. Yellow stars are intermediate states obtained by interpolation.

## 3. Experimental evaluation

Models of four patients with real pelvic fractures of various formats were specifically selected for experimental validation (2 males and 2 females, aged 36, 62, 47, 53 respectively). These CT data were acquired from Beijing Jishuitan Hospital. All the patients received abdominal CT scan. The CT scans were acquired on a Toshiba Aquilion scanner. The average voxel spacing is $0.82 \times 0.82 \times 0.94$ mm$^3$ The average image shape is $480 \times 397 \times 310$. The simulation experiments were performed on a Windows 10 computer with Intel(R) Core(TM) i7–8700 CPU @ 3.20 GHz 3.19GHz. The original CT data in DICOM format were first manually segmented by surgeons with extensive clinical experience and then reconstructed as 3D models with point cloud extraction using software 3DSlicer [44].

The fractures are externally rotated sacroiliac joint dislocation, internally rotated sacral fracture (sacral fragment and iliac are connected), acetabular fracture with displacement of the ischium, and upper and lower pubic ramus fracture with internal rotation of the main iliac fragments respectively. Based on traditional Tile pelvic fracture classification [45], the four fracture types were C1–2, C1–3, A2 and B1. However, in contrast to the tile typing based on the stability of the pelvic ring, the ease of pelvic fracture reduction path planning is dominated by spatial mobility of the displaced bone fragments and the complexity of the surrounding obstacles. Due to the complexity of pelvic fracture, the reduction of major fracture fragment was the primary task of the experiment, with other parts of the pelvis having been moved to the desired anatomical position through previous works [14] and regarded as the fixed part during reduction. With the circumferential morphology of the pelvis, major obstacles for fracture reduction stem from the occlusion of one or both sides of the bone fragments. The above types are labeled as I, II, III and IV, with spatial mobility of the moving fragment from high to low. Based on this, three experiments were devised to verify the effectiveness of proposed method. For each simulation experiment, the same set of parameters was repeated 5 times, and for non-constant parameters such as search time, the mean value was taken as the final result.

Fig. 5

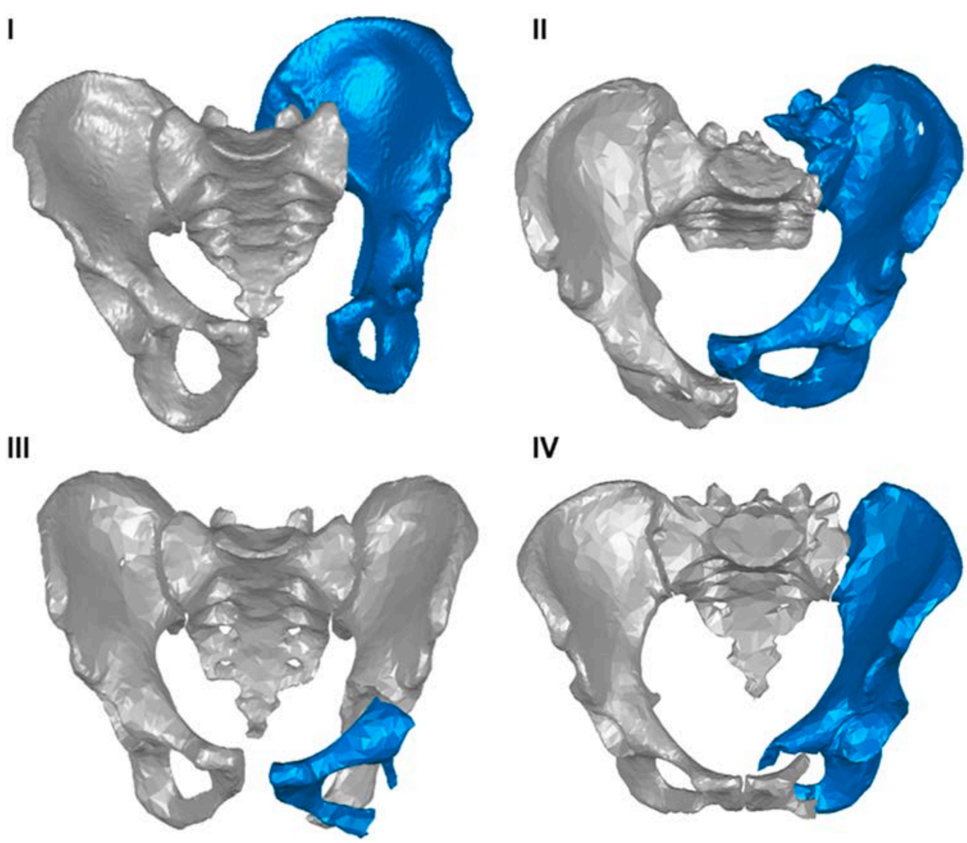


**Fig. 5.** Four pelvic fracture models for simulation experiments. I is externally rotated sacroiliac joint dislocation. II is internally rotated sacral fracture with the connection of sacral fragment and iliac during pre-planning. III is acetabular fracture with displacement of the ischium. IV is upper and lower pubic ramus fracture with internal rotation of the main iliac fragments.

### 3.1. Innovation verification

The validation of optimizations on A* method was implemented first. The experimental results are generated under the premise of keeping the other parts unchanged except the comparison part, including: (1) The efficiency and length of generated path of redirection optimization on translational search. (2) The impact of number of steps *NS* on path search. (3) The impact of *w* on path search. (4) The impact of algorithm restructuring to postdate collision detection on path search. (5) Post smoothing.

The search efficiency of an algorithm is primarily quantified by the search time. For variable control, the search time for comparison is limited to the time needed for path search (part 2.4), and the pre-processing and post-processing time are excluded. The final generated path consists of a series of intermediate states $[S_0, S_1, S_2, \cdots, S_n]$, so the path length $l$ in this study is the sum of distances of the intermediate states in order, which is calculated as follows:

$$l = \sum_{j=1}^{n} \frac{\sum_{i=1}^{num} \left| S_j * [x_i, y_i, z_i] - S_{j-1} * [x_i, y_i, z_i] \right|}{num} \tag{7}$$

Where $S_j{*}[x_i, y_i, z_i]$ is the point of fracture fragment point cloud of state $S_j$, $S_0$ is $S_{start}$ and $S_n$ is $S_{goal}$. The search time and path generation length are calculated consistently throughout simulation experiments.

### 3.2. Comparison on different path planning method

Since translation and rotation are both considered in the planning process, path planning methods that separate translation and rotation are excluded. The generated paths are compared with that of a 3D path planning method with rotationally uniform interpolation along the z-axis [35] and a previously devised semi-automatic path planning method based on a linear planner [29]. Notably, since the fracture fragment is quite close to the other parts in both initial and target positions, the AABB Octree method in 3D planning was no longer applicable and was replaced by the collision detection method on Section 2.3. The same collision detection method allows for better control of variables, thus reflecting the differences between the two methods.

### 3.3. Muscle stretching during reduction

In addition to the avoidance of obstacles between fractures, minimizing damages to the surrounding tissues and avoiding overstretching were also required, so changes in the length of relevant muscles during reduction were observed experimentally. Through relevant researches [46–48], nine groups of muscles, shown in Fig. 6(a), namely gluteus maximus, gluteus medius, gluteus minimus, tensor fasciae latae (together with iliotibial band), iliacus, psoas major, adductor longus, adductor magnus, and biceps femoris longus were ultimately selected as the main muscles during fracture reduction. Since the CT data of the pelvis usually lacked the complete lower limb, the bones of lower limb were moved to the corresponding position by deformation alignment, and then the attachment points of the above muscles were tracked to obtain the real-time length of each muscle. Skeletal muscles around the pelvis were categorized into three types according to their morphology: fusiform, unipennate and pennate muscle, with representative muscles being the biceps femoris longus, gluteus medius, gluteus maximus and psoas major. Fig. 6(b)~(d) shows the calculation of their lengths, with the fusiform is simplified as the length between two muscle attachment points, the unipennate is the average distance between multiple attachment points uniformly selected from one side of the attachment region to a single attachment point on the other side, and the pennate was the average distance between points uniformly taken on both sides along the direction of the muscle fibers. Notably, the iliacus and psoas major muscles wrap around from the anterior side of the pelvis and were therefore resistant to being simplified to a straight line between two attachment points. Therefore wrapping points were chosen to better approximate the length of the muscle, as shown in Fig. 6(e), where one side of the attachment points converges on the wrapping point before connecting to the other side of the attachment point of the muscle. To

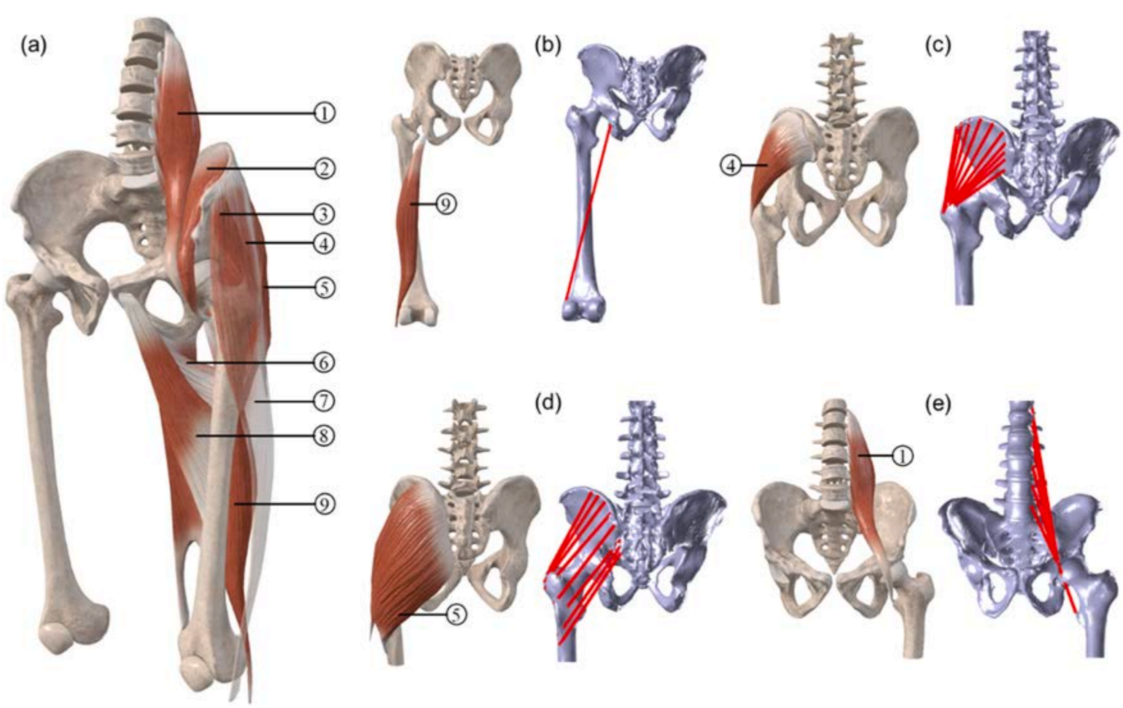


**Fig. 6.** Stretched muscles being observed and calculated during reduction. (a) Muscles considered during fracture reduction. ① to ⑨ are psoas major, iliacus, gluteus minimus, gluteus medius, gluteus maximus, adductor magnus, tensor fasciae latae (together with iliotibial band), adductor longus, and biceps femoris longus respectively. The left side of (b)~(e) shows the muscle morphology of the biceps femoris longus, gluteus medius, gluteus maximus and psoas major, and the right side shows the calculation of their lengths (taking model I as an example). For accurate calculation, the psoas major muscle needs to add a separate wrapping point.

approximate the lower extremity being pulled by a traction device during reduction, the position of the femur was translated with the acetabulum during movement of the fragment, but its rotation posture remained unchanged. Changes of muscle length were calculated and compared for four fractures with different generated path, with III only took adductor longus and adductor magnus into consideration.

## 4. Result and discussion

### 4.1. Redirection optimization of translational search

Shown in Table 2, the computational efficiency and generated path length of uniform interpolation is worth than that of the optimized method, except for the slightly longer generated path of III. This would happen in the case of fractures where the intensive search is in the same direction as the path rounding, which has a lower probability of occurrence. Optimization contributes to the improvement of the search efficiency of the algorithm and has less impact on the length of the generated paths as uniform search in all directions is guaranteed. For I and IV, the optimized search time is only about 1/4 of that of the uniform interpolation due to excessively small travel distances in one direction.

### 4.2. The impact of NS

Table 3 shows the translational step length (rotational step length is close to it), search time and final generated path length for *NS*=10, 15, 20, 30. As *NS* increases, the search step length decreases and the sampling of the search space becomes more intensive, and thus the final path generated by the algorithm are generally shorter, as evidenced by the results of path length. However, the detailed search leads to an increase in computational effort. For model II, the search time of *NS*=30 is 10 times longer than that of *NS*=10, without significant reduction in the path length. For model III, it is >24 times. For balance of search efficiency and search effectiveness, *NS*=15 is chosen as the optimal parameter.

### 4.3. The impact of w

***w*** was tested from 1.0 to 2.0 (at 0.1 interval) to demonstrate its effect on search results. Shown in Fig. 7, the search time first decreases rapidly as the value of *w* increases, and then stabilises after 1.5. When *w*=1, it is a standard heuristic function similar to that of traditional A* method. The search time of each model at *w*=1.5 is about 1/100 ~ 1/800 of that at *w*=1, among which III changes from 13,758.47 s to 17.58 s, and IV changes from 36,438.96 s to 60 .02s. The length of generated path varies inconspicuously before *w*=1.5, and starts to increase gradually after 1.6. When *w*>1, the proportion of the estimated cost $h(n)$ in $f(n)$ of a node increases, so that the nodes closer to the target location has a smaller value of $f(n)$. The goal convergence of the search is intensified with the increase of *w*, which enables higher search efficiency. However, efficient search leads to inevitable detours that is hard to be eliminated by subsequent post smoothing, which makes the length of the generated path increase. Similar to 4.2, to balance the search efficiency and path length, *w*=1.5 is chosen as the optimal value.

**Table 3**
The impact of ***NS*** on path search.

| | NS | 10 | ***15*** | 20 | 30 |
|---|---|---|---|---|---|
| **I** | Translational step length (mm) | 1.93 | ***1.29*** | 0.97 | 0.65 |
| | Path length (mm) | 57.48 | ***54.78*** | 54.14 | 54.24 |
| | Search time (s) | 15.67 | ***26.84*** | 41.25 | 77.64 |
| **II** | Translational step length (mm) | 1.14 | ***0.76*** | 0.57 | 0.38 |
| | Path length (mm) | 29.85 | ***28.45*** | 28.14 | 28.56 |
| | Search time (s) | 188.65 | ***309.63*** | 650.65 | 3282.78 |
| **III** | Translational step length (mm) | 1.27 | ***0.85*** | 0.64 | 0.43 |
| | Path length (mm) | 29.55 | ***28.11*** | 27.73 | 27.81 |
| | Search time (s) | 11.13 | ***17.58*** | 75.49 | 413.17 |
| **IV** | Translational step length (mm) | 0.77 | ***0.51*** | 0.38 | 0.26 |
| | Path length (mm) | 18.69 | ***17.40*** | 17.36 | 17.21 |
| | Search time (s) | 45.03 | ***62.02*** | 80.02 | 117.72 |

### 4.4. Algorithm restructuring

From Table 4, it is visible that the restructuring of the algorithm has no impact on the process and results of the search, but its collision detection time is greatly reduced, which leads to significant decrease in the search time to about 1/12 to 1/3 of the traditional method. The traditional algorithm performs collision detection on the expanded child nodes initially and selects all non-collision child nodes for subsequent operations. Nevertheless, not all 80 child nodes obtained through expansion are selected for further expansion, and the collision detection of unselected nodes is undesirable. While specific collision detection method has been applied in this study, it still requires substantial computational effort. Therefore, the improved method postpones the collision detection and performs it after the child node is selected to be expanded, which reduces the number of collision detections to about 1/10 of the original one and thus improves the search efficiency.

### 4.5. Post smoothing

From Section 4.2, *w*=1.5 improves the search efficiency, but also generates redundant paths and makes it longer. After post smoothing, the curved path is straightened and shortened, thus breaking the limitations of grid search. Shown in Fig. 8 and Table 5, the smoothed path not only reduces the length by 10 %~15 %, but also greatly reduces the number of turns, which meets the moving requirements of the surgical robot.

### 4.6. Results on different method

The proposed method was compared with 3D augmented A* in [36], and Semi-automatic method based on linear planner in our previous work [29]. While the 3D augmented A* takes rotational DOF into consideration, it associates the rotational DOF with Z-axis rather than adding it as a separate DOF to the path search. Due to the low DOFs, this method is applicable for cases with large movable space for bone

**Table 2**
Comparison between uniform interpolation and redirection optimization.

| | | Each translational direction length(mm) | Nodes in Close List | Nodes in Collision List | Path length (mm) | Search time (s) |
|---|---|---|---|---|---|---|
| **I** | Uniform Interpolation | [0.07,1.97,1.07] | 68 | 369 | 56.67 | 98.84 |
| | Optimized | ***1.29*** | ***25*** | ***94*** | ***54.78*** | ***26.84*** |
| **II** | Uniform Interpolation | [0.62,0.70,0.93] | 303 | 880 | 28.61 | 543.78 |
| | Optimized | ***0.76*** | ***211*** | ***606*** | ***28.45*** | ***309.63*** |
| **III** | Uniform Interpolation | [1.24,0.46,0.65] | 26 | 131 | 27.98 | 26.15 |
| | Optimized | ***0.85*** | ***23*** | ***99*** | ***28.01*** | ***17.58*** |
| **IV** | Uniform Interpolation | [0.58,0.66,0.13] | 264 | 376 | 17.79 | 246.38 |
| | Optimized | ***0.51*** | ***33*** | ***128*** | ***17.40*** | ***60.02*** |

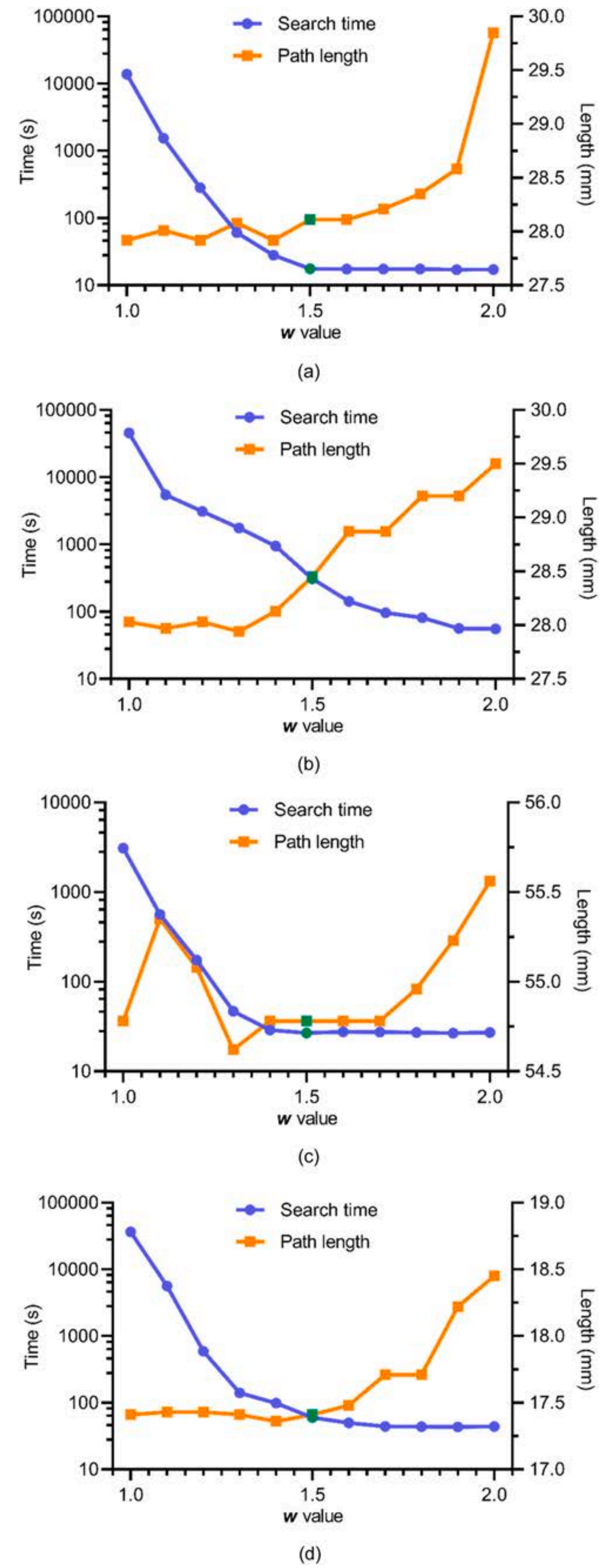


**Fig. 7.** Impact of different $w$ on path search. (a)~(d) represent the results of Models I to IV, respectively. The green dots are the results for $w = 1.5$ chosen in this algorithm.

**Table 4**
Comparison of search results before and after algorithm restructuring.

| | | Nodes in Close List | Nodes in Collision List | Path length (mm) | Search time (s) |
|---|---|---|---|---|---|
| **I** | Traditional method | 25 | 1427 | 54.78 | 218.81 |
| | Improved method | ***25*** | ***94*** | ***54.78*** | ***26.84*** |
| **II** | Traditional method | 211 | 2754 | 28.45 | 840.56 |
| | Improved method | ***211*** | ***606*** | ***28.45*** | ***309.63*** |
| **III** | Traditional method | 23 | 1145 | 28.11 | 119.30 |
| | Improved method | ***23*** | ***95*** | ***28.11*** | ***17.58*** |
| **IV** | Traditional method | 33 | 1388 | 17.40 | 551.62 |
| | Improved method | ***33*** | ***128*** | ***17.40*** | ***62.02*** |

fragments, as in I and II. For III and IV, no feasible paths could be obtained. Shown in Fig. 9, the proposed method outperforms the other two in terms of path length and computation time. The proposed method is about 90 % of 3D augmented A* and 40 %~70 % of semi-automatic methods in terms of path length. The superiority of the method in search time is more significant, with 6 %~25 % of 3D augmented A* and about 7 % of semi-automatic method (36 % for II). Fig. 10 shows the generated path for four pelvic fracture models based on different methods. The paths resulting from the proposed algorithm are smoother and closer to curves, and the number and angle of turns are smaller compared to the 3D augmented A* method. The results of semi-automatic planning method are consistent with the manual reduction process of surgeons which is the steps of 'distraction-alignment-translation-close'. Therefore, significant path redundancy exists in the semi-automatic paths, and the path length is the longest. As a complement to the reduction path line in Fig. 10, the attached videos (Model_I.mp4, Model_II.mp4, Model_III.mp4 and Model_IV.mp4) could better demonstrate the rounding of the fractured bone and its own pose changes as it moves. For better visualization of the 3D path, different views of the pelvis are shown in the video, including inlet anteroposterior projection, outlet anteroposterior projection and overview of the pelvis.

### *4.7. Changes of muscle stretching on different paths*

Shown in Fig. 11–14, the muscle stretching along the path generated by the proposed algorithm is smoother compared to the other two methods. Through taking rotation as a separate search DOF with redirection of uniform translation, the proposed algorithm has a relatively homogeneous change of movement for each search step. The 3D augmented A* method binds rotation to the Z-axis, so that movement of the model along Z-axis produces simultaneous rotational motion, resulting in more pronounced muscle stretches, especially for larger translation distance on the Z-axis. For semi-automatic paths, the muscle stretch changes are more complex and may even be dramatic due to the rough manual planning of obstacle avoidance.

Since muscle force normally proportional to muscle length, the calculation of force doing work was simulated by integrating and summing the length change of muscles with integrating value of muscle stretch greater than 0. Due to the large path redundancy, semi-automatic paths are significantly higher than the other two methods. Fig. 15 shows that the integrating value of the proposed method is about 90 % of that of 3D augmented A* method. Therefore, the proposed method better satisfy clinical requirements of fracture reduction with stable muscle stretching and lower muscle doings.

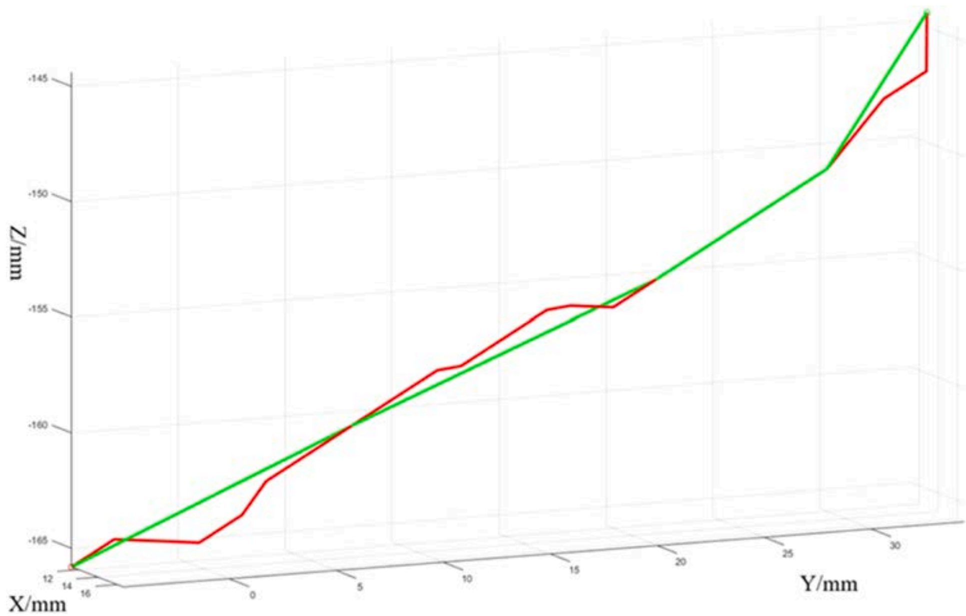


**Fig. 8.** The path before and after post smoothing. The red line is the initial path before smoothing with many turns. The green line is the final path after smoothing.

**Table 5**
The effect of post smoothing.

| | | Path length (mm) | Number of turns |
|---|---|---|---|
| **I** | Before | 61.01 | 13 |
| | After | ***54.78*** | ***2*** |
| **II** | Before | 32.72 | 10 |
| | After | ***28.45*** | ***4*** |
| **III** | Before | 31.44 | 14 |
| | After | ***28.11*** | ***4*** |
| **IV** | Before | 19.94 | 12 |
| | After | ***17.40*** | ***3*** |

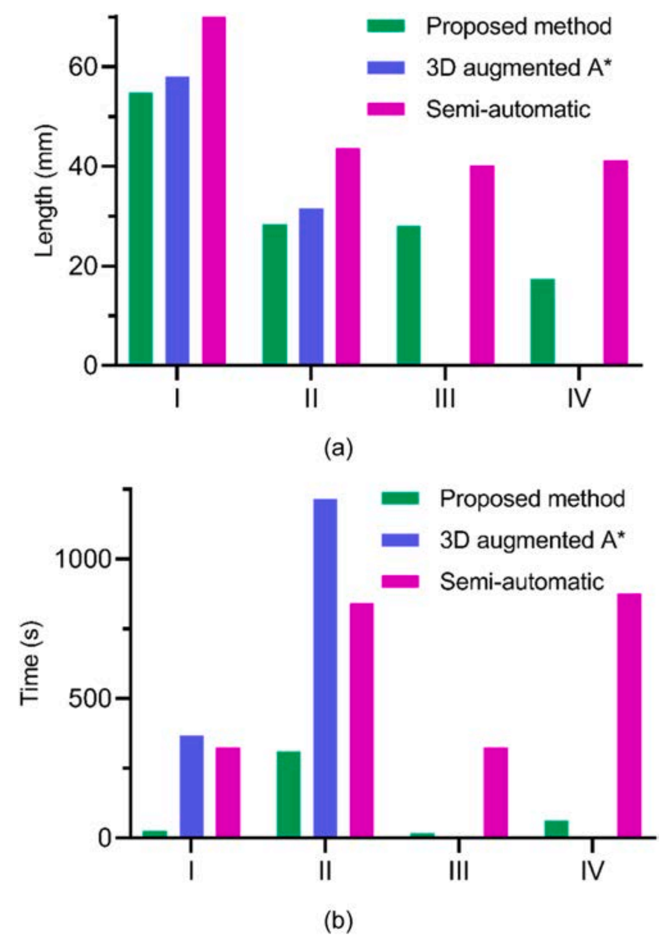


**Fig. 9.** Contrast of results generated by different methods. (a) Path length generated by different methods. (b) Search time by different methods.

## 5. Discussion

### *5.1. Analysis on simulation results*

Conventional preoperative planning for pelvic fracture reduction emphasizes on high-precision reconstruction of the fractured pelvis, with minimal consideration on how to move the displaced bone fragments to the target location. To address this, an automatic path planning algorithm that incorporates both translation and rotation is proposed. Through separately defined search direction of rotating around $\overrightarrow{\boldsymbol{RV}}$, the search could cover both translational and rotational degrees of freedom, thereby allowing fracture fragments to rotate around obstacles. As shown in Fig. 10(b), since the rotation is a separate degree of freedom, the fracture fragments are more flexible without detouring around far to reach the target position through obstacles, the path generated in this study is shorter and smoother compared to the 3D augmented A* method, which adapts the requirements of robotic locomotion and clinical fracture reduction. The translational redirection and optimization of the structure of the improved algorithm (including adjustment on heuristic function and algorithm architecture) designed for the high-dimensional search efficiency problem of the traditional A* algorithm reduces the search time to 1/100~1/1000, while the final path length after smoothing post-processing has no significant increase, which realizes the balance between search efficiency and search effectiveness of the algorithm.

The avoidance of secondary intraoperative injuries is an important consideration for clinicians. It is generally believed that less movement of the injured site and pulling of tissues around the incision result in lower intraoperative risk of secondary injuries and faster postoperative recovery of the patient [49,50]. Through the Table 4 and Fig. 10(a)(b), the smoothing post-processing makes the final generated path consist of

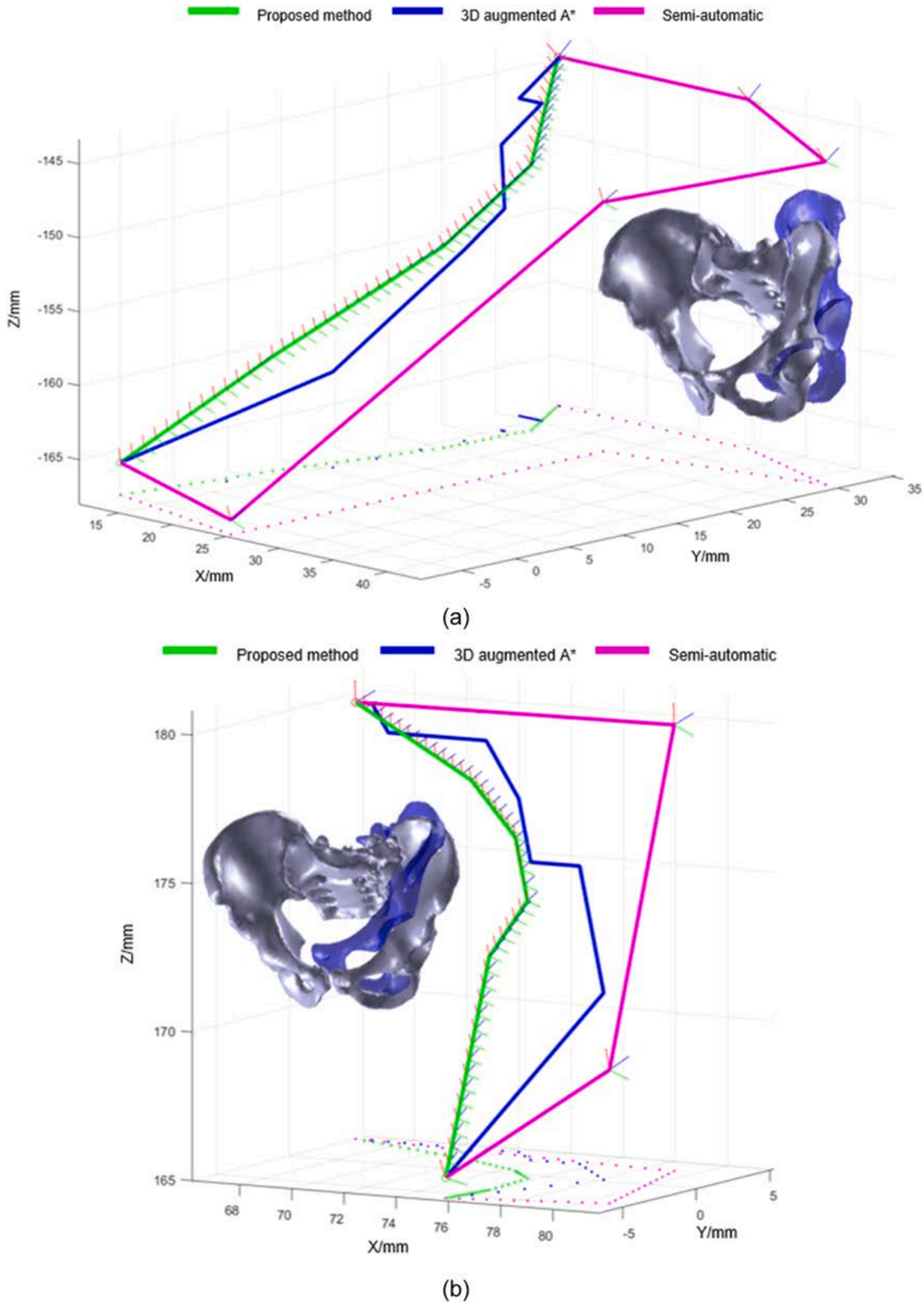


**Fig. 10.** Paths generated by different methods. (a)~(d) are the path planning results for model I to IV, respectively. The green, blue and pink lines are the results of the proposed method, 3D augmented A* method and semi-automatic method. The red, blue and green arrows are utilized to show the rotational pose of the model at that position.

only several intermediate nodes with low variability. Combined with the high degree of freedom for flexible bending, this enables smoother muscle stretching state changes at only a few nodes. In contrast, the 3D augmented A* algorithm generates paths with large number of turning nodes with high turning angles (Figs. 11 and 12). Semi-automatic path planning methods are more obvious than 3D augmented A* in this

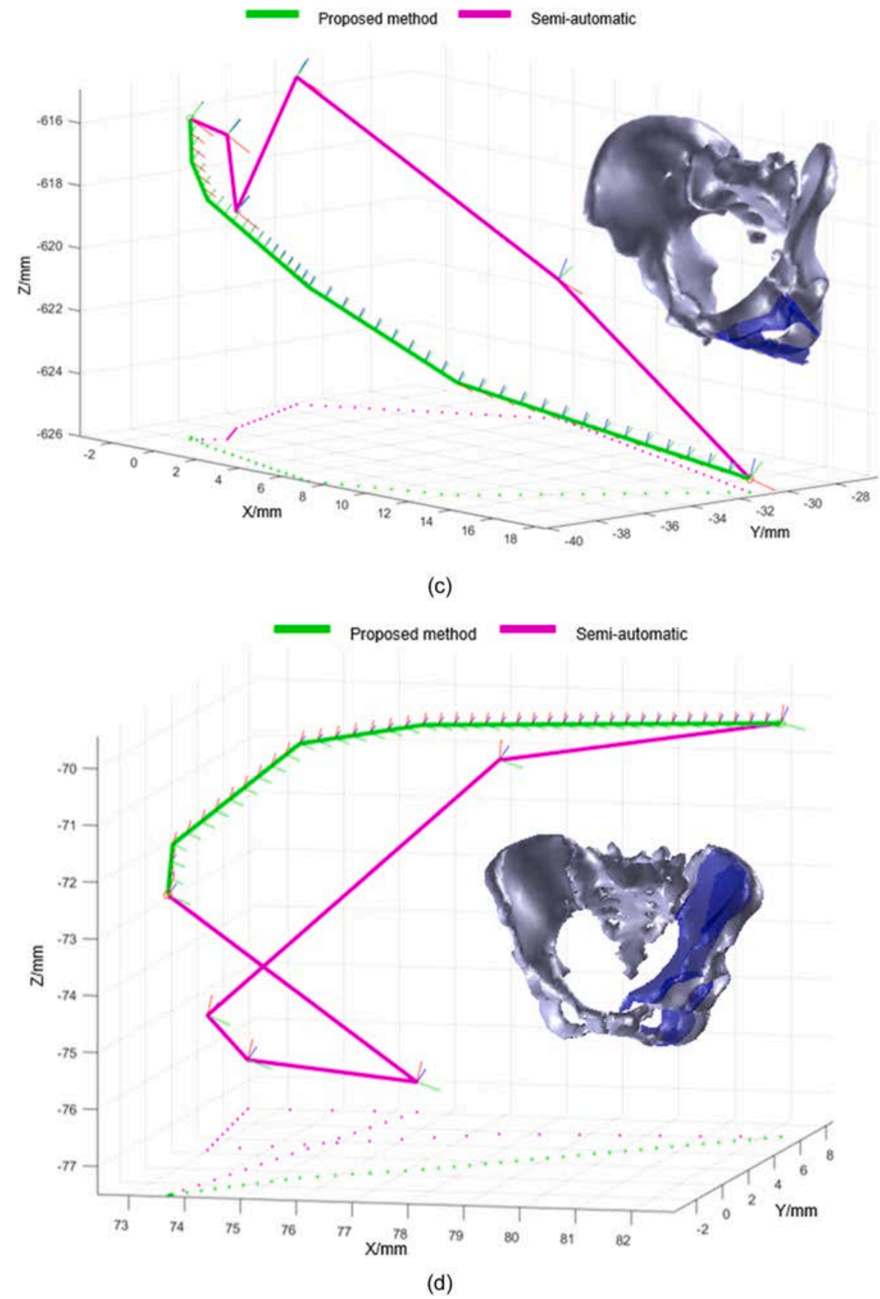


**Fig. 10.** (*continued*).

respect. Thus the path generated based on multi degree of freedom planning has a shorter path length with smoother muscle stretching and lower total muscle stretching, which meets the clinical safety requirements. As the first known path planning method for fracture reduction that considers rotation as a separate DOF in the path search, it outperforms previous 3D methods and semi-automatic methods in terms of collision detection, path length and smoothness, search time, and surrounding tissue stretching conditions.

With the circumferential morphology of the pelvis, the ease of pelvic fracture reduction path planning is dominated by spatial mobility of the displaced bone fragments and the complexity of the obstacles on one or both sides. On this basis, four pelvic fracture types that included different fracture locations together with fracture reduction occlusion scenarios were selected specifically, that is, unilateral occluded without fracture line (model I),unilateral occluded restoration with fracture line (model III), and bilateral occluded restoration with fracture line (models II and IV corresponding to different rotational situations).In contrast to previous pelvic fracture reduction algorithms using only sacroiliac joint dislocations for testing [35,36], the fracture types selected for this study were more comprehensive, containing sacroiliac joint dislocations, sacral fractures, and iliac fractures, and taking both internal and external rotation of the fracture into account. The models for experiments include multiple pelvic fractures that are applicable to pelvic fracture reduction robots, expanding the indications available for reduction path planning.

### 5.2. Limitations and future works

The study is based on the classical A* algorithm, which is capable of obtaining the optimal unique path in the searched through sufficient computation. However, the curse of dimensionality problem of the algorithm is not resolved completely and the computational time required

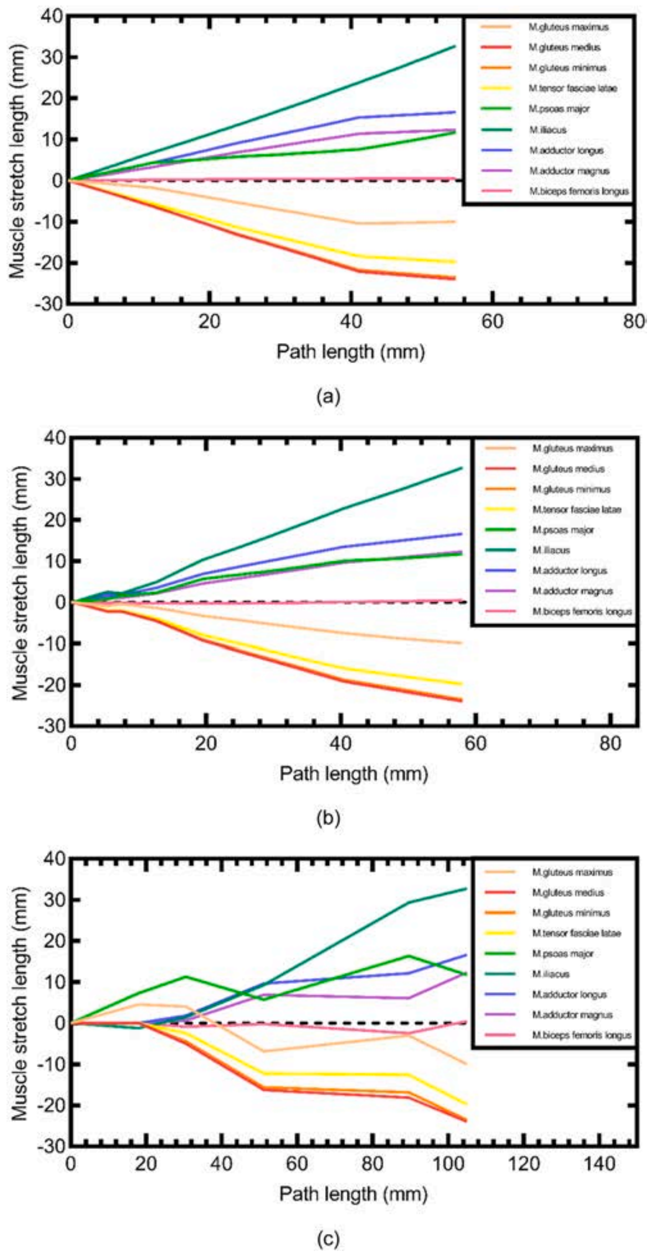


**Fig. 11.** Variation in length of different muscle stretches during fracture reduction of model I. (a) Proposed method. (b) 3D augmented A* method. (c) Semi-automatic method.

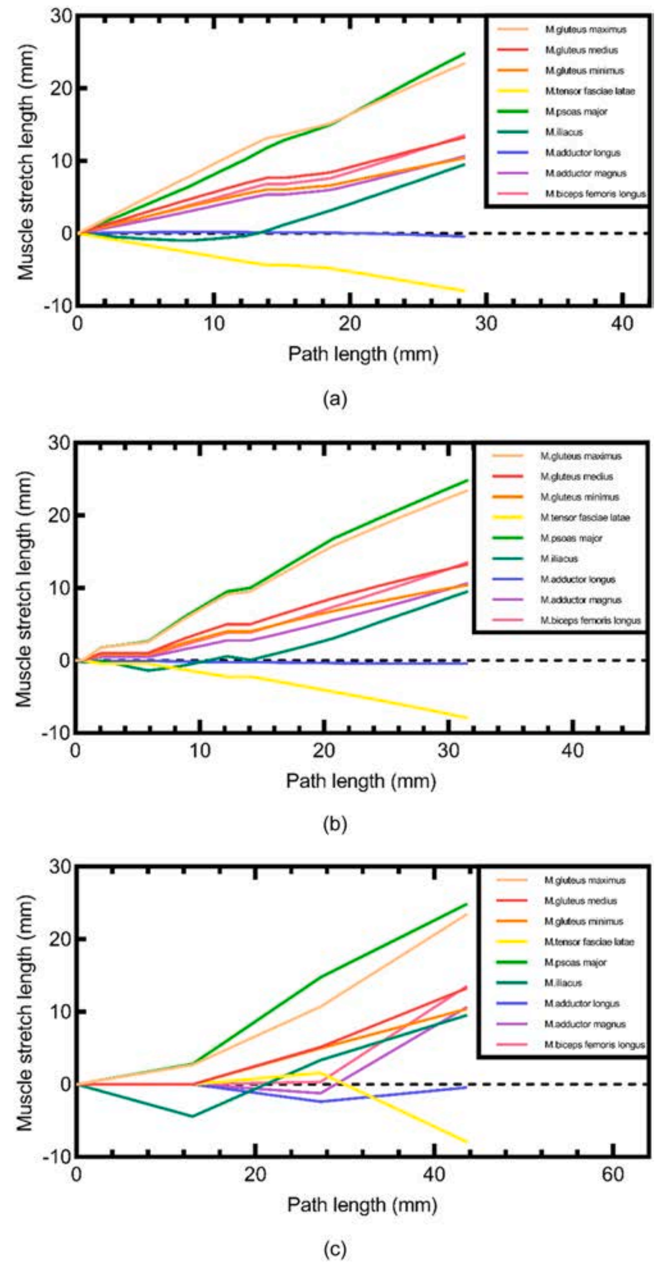


**Fig. 12.** Variation in length of different muscle stretches during fracture reduction of model II. (a) Proposed method. (b) 3D augmented A* method. (c) Semi-automatic method.

by the algorithm still increases sharply as the computational dimensionality rises [34]. Only one-dimensional rotation DOF was added to the path search in this study, and the optimized computational efficiency is acceptable. Since intraoperative traction provides sufficient movement space for pelvic fracture reduction, 4 DOF path planning has been verified to satisfy common robotic fracture reduction surgeries, but there are still complex fracture scenarios that are difficult to obtain reduction path. This type of fracture requires higher dimensional path planning solutions. Sampling-based and intelligent path planning methods [30–32] will be introduced in the future to realize higher DOF path planning and to balance computational time with computational efficiency.

On the other hand, the collision-free path planning method based on this paper only considers the geometry of the bone fragments and is suitable for preoperative planning. The generated reduction path could be impractical in clinical application due to resistance of the surrounding soft tissues and small bone fragments that might be neglected in the three-dimensional reconstruction. Repetitive waiting for the re-planned path might be unacceptable. In addition, testing for changes in stretch of the surrounding tissues was simple, with only the muscle stretch length was calculated instead of the muscle force. The stretching forces generated by different muscles may be superimposed or cancelled with each other due to their different attachment sites. For such issues, an in vivo simulation platform for pelvic fracture is required in further research [36,48], where musculoskeletal models suitable for pelvic fracture are designed to simulate the reduction force and incorporated into the subsequent reduction path planning to make the generated preoperative path more relevant to the in vivo scenario. In addition, intelligent strategies based on reinforcement learning will also be considered in our future study [51,52], which is capable of responding to intraoperative emergencies unconsidered preoperatively through strategy learning to guarantee the safety of the reduction

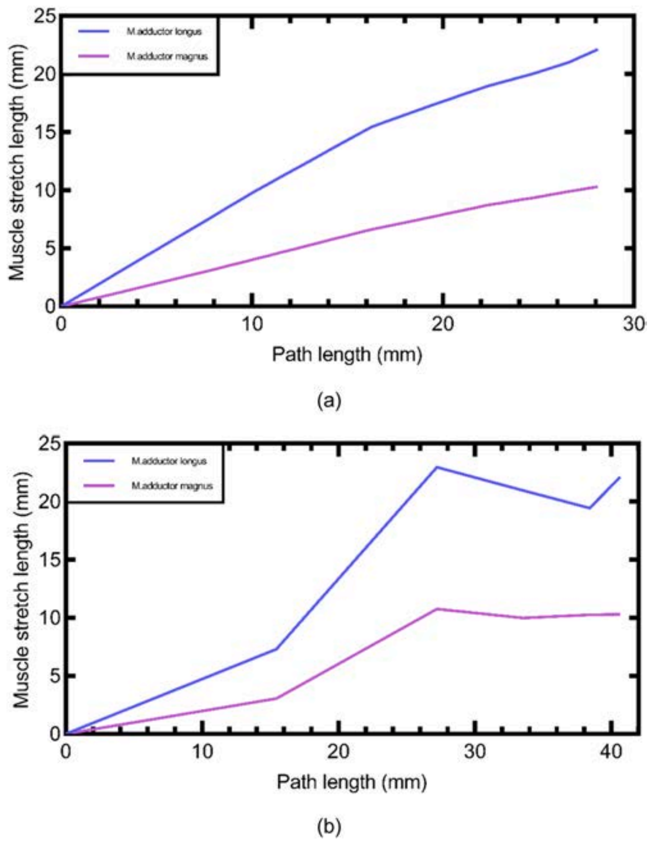


**Fig. 13.** Variation in length of different muscle stretches during fracture reduction of model III. (a) Proposed method. (b) Semi-automatic method.

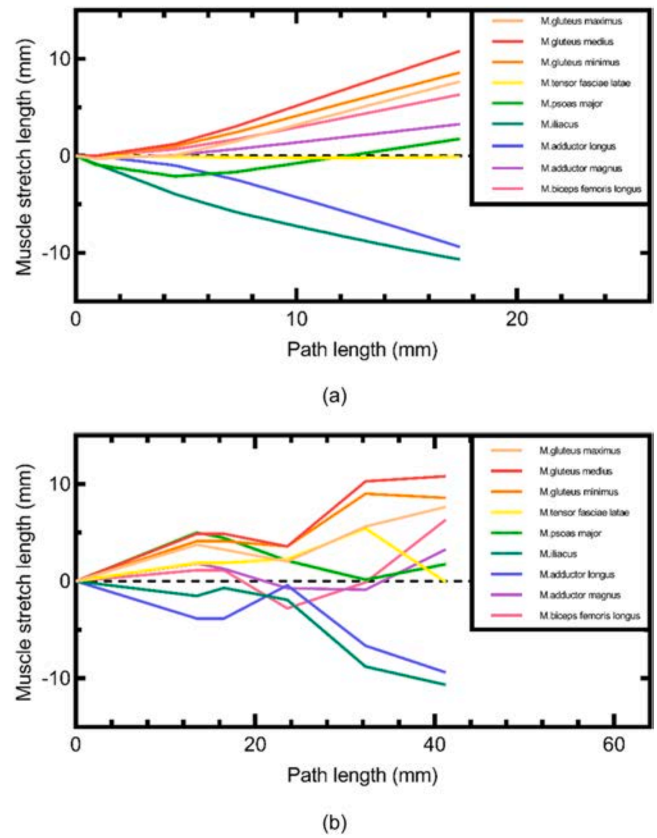


**Fig. 14.** Variation in length of different muscle stretches during fracture reduction of model IV. (a) Proposed method. (b) Semi-automatic method.

process.

Expansion of the indications and in vivo study are also part of further works. As preliminary research of multi-degree-of-freedom path planning, it only takes the cases of single bone fragment displacement into consideration, with the other bone fragments moved to the desired anatomical position by default. However, in the presence of multiple large bone fragments, preoperative planning requires consideration of the effect of the motion of individual fragments on surrounding fragments, and the sequence of the fragments motion is also an essential part of planning. Based on the proposed method, the reduction sequence of the fragments could be programmed manually by surgeons and thereby generating a preoperative scheme with reduction paths. Incremental sampling-based task and motion planners [53] for multiple bone fragments will also be considered to solve this problem automatically. Simulation models are challenging in matching realistic clinical patient scenarios given the complex human pelvic structure and individualized differences in injuries, thus in vivo studies are essential. In further work, experiments will be implemented in collaboration with the developed pelvic fracture repositioning robot to investigate the specific problems encountered in clinical applications.

## 6. Conclusion

The article described a solution for the definition of feasible pathways for robotically actuated reduction operation in a pelvic fracture surgical scenario, which represents a typical example of volumetric object movement in dense environment characterized by narrow spaces. Specialized collision detection method based on bounding sphere hierarchy enables fast and precise testing. Rotational alignment operations are incorporated into path search by including rotation around the specified axis as a separate degree of freedom. Translational redirection and the optimized Lazy A* algorithm facilitate the generation of initial paths. The final post smoothing procedure further smoothes and shortens the path. Various pelvic fracture models validate the applicability and superiority of the proposed method. The optimized algorithm reduces the search time to 1/100~1/1000 without a significant increase in the final path length, achieving a balance between search efficiency and search effectiveness. Meanwhile, the muscle stretching condition of the path generated is also optimal compared to other methods.

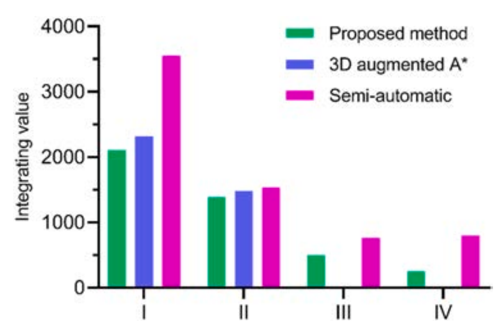


**Fig. 15.** Integrating value of the length change of muscles during reduction based on different method.

Future work attempts to further enhance the search DOFs to accommodate more complex fracture scenarios. Moreover, personalized pelvic fracture biomechanical models as well as continuous collision detection algorithms are required for subsequent better planning. The feasibility of the planned paths should also be in vivo validated in further experiments.

## Ethics statement

This study followed all applicable international and national ethical regulations. For studies involving humans or animals, we have obtained the necessary ethical approvals (No.202203–91 of Beijing Jishuitan Hospital, the approval was granted in March 2022) and ensured informed consent from all participants.

- For studies involving humans: we have ensured that all participants have provided written informed consent and have the right to withdraw from the study at any time. Research data are collected and processed in accordance with privacy protection principles, and all personally identifiable information is deleted or encrypted.

- For studies involving animals: We have followed internationally recognized ethical guidelines for animal experimentation and have ensured that the animals have received proper care and minimal suffering during the study.

We promise that the results of this study will be reported in an honest, objective and responsible manner and will not be modified or manipulated in any way that could mislead readers or compromise the integrity of the study.

## CRediT authorship contribution statement

**Chao Shi:** Writing – review & editing, Writing – original draft, Visualization, Validation, Supervision, Software, Data curation. **Qing Yang:** Writing – original draft. **Yuantian Wang:** Validation. **Xiangrui Zhao:** Software. **Shuchang Shi:** Methodology. **Lijia Zhang:** Methodology. **Sutuke Yibulayimu:** Methodology, Investigation. **Yanzhen Liu:** Methodology, Investigation. **Chendi Liang:** Data curation. **Yu Wang:** Writing – review & editing, Writing – original draft, Visualization, Validation, Software, Methodology, Data curation. **Chunpeng Zhao:** Data curation.

## Declaration of competing interest

All authors declare that they have no conflict of interest.

## Acknowledgments

This research is supported by the Beijing Science and Technology Project (Z201100005420033, Z221100003522007) and the Natural Science Foundation of Beijing (L222136, L212055, L222057).

All authors declare that they have no conflict of interest.

## Supplementary materials

Supplementary material associated with this article can be found, in the online version, at doi:10.1016/j.cmpb.2025.108591.

## References

[1] Burkhardt, M., Kristen, A., Culemann, U., et al. Pelvic fracture in multiple trauma: are we still up-to-date with massive fluid resuscitation? Injury, 45 Suppl 3 (2014): S70–S75. doi: 10.1016/j.injury.2014.08.021.

[2] B.J. Eastridge, A. Starr, J.P. Minei, et al., The importance of fracture pattern in guiding therapeutic decision-making in patients with hemorrhagic shock and pelvic ring disruptions, J. Trauma Acute Care Surgery 53 (3) (2002) 446–451.

[3] P.R. Miller, P.S. Moore, E. Mansell, et al., External fixation or arteriogram in bleeding pelvic fracture: initial therapy guided by markers of arterial hemorrhage, J. Trauma Acute Care Surgery 54 (3) (2003) 437–443, https://doi.org/10.1097/01.TA.0000053397.33827.DD.

[4] S.J. Pereira, D.P. O'brien, F.A. Luchette, et al., Dynamic helical computed tomography scan accurately detects hemorrhage in patients with pelvic fracture, Surgery. 128 (4) (2002) 678–685, https://doi.org/10.1067/msy.2000.108219.

[5] S.E. Putnis, et al., Open reduction and internal fixation of a traumatic diastasis of the pubic symphysis: one-year radiological and functional outcomes, J. Bone Joint Surgery-Br., 93 (1) (2011) 78–84, https://doi.org/10.1302/0301-620X.93B1.23941.

[6] S. Takashi, et al., Long-term functional outcome after unstable pelvic ring fracture, J. Teauma 63 (4) (2007) 884–888, https://doi.org/10.1097/01.ta.0000235888.90489.fc.

[7] Y. Kokubo, H. Oki, D. Sugita, et al., Functional outcome of patients with unstable pelvic ring fracture: comparison of short- and long-term prognostic factors, J. Orthopaed. Surgery 25 (1) (2017) 2309499016684322, https://doi.org/10.1177/2309499016684322.

[8] D. Raabe, S. Dogramadzi, R. Atkins, Semi-automatic percutaneous reduction of intra-articular joint fractures-An initial analysis, in: IEEE International Conference on Robotics and Automation, IEEE, 2012, pp. 2679–2684, https://doi.org/10.1109/ICRA.2012.6225076.

[9] G. Dagnino, I. Georgilas, P. Köhler, R. Atkins, S. Dogramadzi, Image-based robotic system for enhanced minimally invasive intra-articular fracture surgeries, in: 2016 IEEE International Conference on Robotics and Automation (ICRA), IEEE, 2016, pp. 696–701.

[10] J.J. Jiménez-Delgado, F. Paulano-Godino, R. PulidoRam-Ramírez, J.R. Jiménez Pérez, Computer-assisted preoperative planning of bone Ffracture reduction: simulation techniques and new trends, Med. Image Anal. 30 (2016) 30–45, https://doi.org/10.1016/j.media.2015.12.005.

[11] C. Wang, B. Connolly, de Oliveira Lopes, et al., Pelvis segmentation using multi-pass U-Net and iterative shape estimation, in computational methods and clinical applications in musculoskeletal imaging. 6th International Workshop, MSKI 2018, Held in Conjunction with MICCAI 2018, Springer International Publishing, Granada, Spain, 2019, pp. 49–57, https://doi.org/10.1007/978-3-030-11166-3_5. September 16, 2018Revised Selected Papers 6.

[12] P. Liu, H. Han, Y. Du, et al., Deep learning to segment pelvic bones: large-scale CT datasets and baseline models, Int. J. Comput. Assisted Radiol. Surg. 16 (2021) 749–756, https://doi.org/10.1007/s11548-021-02363-8.

[13] Y.Z. Liu, Y. Sutuke, Y. Sang, et al., Pelvic Fracture Segmentation Using a Multi-scale Distance-Weighted Neural Network, MICCAI (9) (2023) 312–321, https://doi.org/10.1007/978-3-031-43996-4_30.

[14] Y. Sutuke, Y.Z. Liu, Y. Sang, et al., Pelvic fracture reduction planning based on morphable models and structural constraints, MICCAI (9) (2023) 322–332, https://doi.org/10.1007/978-3-031-43996-4_31.

[15] J. Buschbaum, R. Fremd, T. Pohlemann, A Kristen, Introduction of a computer-based method for automated planning of reduction paths under consideration of simulated muscular forces, Int. J. Comput. Assisted Radiol. Surg. 12 (1) (2017) 369–1381, https://doi.org/10.1007/s11548-017-1562-0.

[16] C. Zhao, M. Guan, C. Shi, et al., Automatic reduction planning of pelvic fracture based on symmetry, Comput. Methods Biomechanics Biomed. Eng. Imaging Vis. 10 (6) (2022) 577–584, https://doi.org/10.1080/21681163.2021.2012830.

[17] R. Han, A. Uneri, R.C. Vijayan, et al., Fracture reduction planning and guidance in orthopaedic trauma surgery via multi-body image registration, Med. Image Anal. 68 (2021) 101917, https://doi.org/10.1016/j.media.2020.101917.

[18] Y. Ge, C. Zhao, Y. Wang, X. Wu, Robot-assisted autonomous reduction of a displaced pelvic fracture: a case report and brief literature review, J. Clin. Med 11 (6) (2022) 1598, https://doi.org/10.3390/jcm11061598.

[19] W.Y. Kim, S.Y. Ko, Hands-on robot-assisted fracture reduction system guided by a linear guidance constraints controller using a pre-operatively planned goal pose, Int. J. Med. Robotics Comput. Assisted Surg. 15 (2) (2019) e1967, https://doi.org/10.1002/rcs.1967.

[20] C. Bignardi, M. Terzini, A.L. Audenino, et al., Pelvic manipulator for fractures reduction, Int. J. Mech. Eng. Technol. 9 (3) (2018) 570–580.

[21] G. Dagnino, I. Georgilas, S. Morad, et al., RAFS: a computer-assisted robotic system for minimally invasive joint fracture surgery, based on pre-and intraoperative imaging, in: 2017 IEEE International Conference on Robotics and Automation (ICRA), IEEE, 2017, pp. 1754–1759.

[22] G. Dagnino, I. Georgilas, S. Morad, et al., Image-guided surgical robotic system for percutaneous reduction of joint fractures, Ann. Biomed. Eng. 45 (2017) 2648–2662, https://doi.org/10.1007/s10439-0171901-x.

[23] G. Dagnino, I. Georgilas, S. Morad, et al., Intraoperative fiducial-based CT/fluoroscope image registration framework for image-guided robot-assisted joint fracture surgery, Int. J. Comput. Assisted Radiol. Surg. 12 (2017) 1383–1397, https://doi.org/10.1007/s11548-017-1602-9.

[24] R. Westphal, S. Winkelbach, T. Gösling, et al., Automated robot assisted fracture reduction, Adv. Robotics Res. Theory Implement. Appl. (2009) 251–262.

[25] R. Westphal, S. Winkelbach, F. Wahl, et al., Robot-assisted long bone fracture reduction, Int. J. Robotics Res. 28 (10) (2009) 1259–1278, https://doi.org/10.1177/0278364909101189.

[26] H. Du, L. Hu, C. Li, et al., Preoperative trajectory planning for closed reduction of long-bone diaphyseal fracture using a computer-assisted reduction system, Int. J. Med. Robot. Comput. Assisted Surg. 11 (1) (2015) 58–66, https://doi.org/10.1002/rcs.1573.

[27] H. Du, L. Hu, C. Li, T. Wang, et al., Advancing computer-assisted orthopaedic surgery using a hexapod device for closed diaphyseal fracture reduction, Int. J. Med. Robot. Comput. Assisted Surg. 11 (3) (2015) 348–359, https://doi.org/10.1002/rcs.1614.

[28] R. Ye, Y. Chen, Path planning for robot assisted femur shaft fracture reduction: a preliminary investigation, in: 2009 IEEE International Conference on Virtual Environments, Human-Computer Interfaces and Measurements Systems, IEEE, 2009, pp. 113–117, https://doi.org/10.1109/VECIMS.2009.5068876.

[29] C. Shi, X. Zhao, X. Wu, C. Zhao, G. Zhu, S. Shi, et al., Real-time 3D navigation-based semi-automatic surgical robotic system for pelvic fracture reduction, in: 2021 IEEE/RSJ International Conference on Intelligent Robots and Systems (IROS), IEEE, 2021, pp. 9498–9503, https://doi.org/10.1109/IROS51168.2021.9636647.

[30] A. Vagale, R. Oucheikh, R.T. Bye, et al., Path planning and collision avoidance for autonomous surface vehicles I: a review, J. Mar. Sci. Technol. (4) (2021) 26, https://doi.org/10.1007/s00773-020-00787-6.

[31] H. Qin, S. Shao, T. Wang, et al., Review of autonomous path planning algorithms for mobile robots, Drones 7 (2023) 211, https://doi.org/10.3390/drones7030211.

[32] U. Ozturk, M. Akdag, T. Ayabakan, A review of path planning algorithms in maritime autonomous surface ships: navigation safety perspective, Ocean Eng. (2022) 251, https://doi.org/10.1016/j.oceaneng.2022.111010.

[33] P.E. Hart, Nils J. Nilsson, B. Raphael, A formal basis for the heuristic determination of minimum cost paths, IEEE Trans. Syst. Sci. Cybernet. 4 (2) (1968) 100–107.

[34] M.L. Muhammed, E.H. Flaieh, Amjad J. Humaidi, Embedded system design of path planning for planar manipulator based on chaos A* algorithm with known-obstacle environment, J. Eng. Sci. Technol. 17 (6) (2022) 4047–4064.

[35] H. Xu, J. Lei, L. Hu, L. Zhang, Constraint of musculoskeletal tissue and path planning of robot-assisted fracture reduction with collision avoidance, Int. J. Med. Robotics Comput. Assisted Surg. 18 (2) (2022) e2361, https://doi.org/10.1002/rcs.2361.

[36] M. Pan, Y. Chen, Z. Li, et al., Autonomous path planning for robot-assisted pelvic fracture closed reduction with collision avoidance, Int. J. Med. Robotics Comput. Assisted Surg. 19 (2) (2023) e2483, https://doi.org/10.1002/rcs.2483.

[37] Y. Chen, M.Z. Pan, Z. Li, et al., Autonomous path planning with muscle force optimization for robot assisted pelvic fracture closed reduction, IEEE Trans. Med. Robot. Bionics 5 (2023) 253–264, https://doi.org/10.1109/tmrb.2023.3265719.

[38] A. Favaro, A. Segato, F. Muretti, et al., An Evolutionary-Optimized Surgical Path Planner for a Programmable Bevel-Tip Needle, IEEE Trans. Robot. (2021) 4, https://doi.org/10.1109/TRO.2020.3043692.

[39] A. Segato, F. Calimeri, I. Testa, et al., A hybrid inductive learning-based and deductive reasoning-based 3-D path planning method in complex environments, Auton. Robots 46 (5) (2022) 645–666, https://doi.org/10.1007/s10514-022-10042-z.

[40] Y. Zhang, D. Luo, J. Li, J.S. Li, Study on collision detection and force feedback algorithm in virtual surgery, J. Healthc. Eng. (2021), https://doi.org/10.1155/2021/6611196.

[41] H.J. Zhao, M.J. Cheng, J.Y. Huang, et al., A virtual surgical prototype system based on gesture recognition for virtual surgical training in maxillofacial surgery, Int. J. Comput. Assist. Radiol. Surg. (2022) 1–11, https://doi.org/10.1007/s11548-022-02790-1.

[42] M.J. Cheng, Y. Zhuang, H.J. Zhao, M. Li, et al., Development of a maxillofacial virtual surgical system based on biomechanical parameters of facial soft tissue, Int. J. Comput. Assist. Radiol. Surg. 17 (2022) 1201–1211, https://doi.org/10.1007/s11548-022-02657-5.

[43] C. Shi, Q. Yang, X.R. Zhao, et al., Fast and precise collision detection for detailed and complex physiological structures, Comput. Methods Programs Biomed. (2023), https://doi.org/10.1016/j.cmpb.2023.107707, 240107707-107707.

[44] A. Fedorov, R. Beichel, J. Kalpathy-Cramer, et al., 3D Slicer as an image computing platform for the Quantitative Imaging Network, Magn. Reson. Imaging 30 (9) (2012) 1323–1341.

[45] M. Tile, Pelvic ring fractures: should they be fixed? The J. Bone Joint Surgery Br. Vol. 70 (1) (1988) 1–12.

[46] E. Esmat, N. Vasilije, Matejčić, et al., Analysis of Muscle Forces Acting on Fragments in Pelvic Fractures, Coll. Antropol. 33 (4) (2009) 1095–1101, https://doi.org/10.2753/CSA0009-4625420204.

[47] A.T.M. Phillips, P. Pankaj, C.R. Howie, et al., Finite element modelling of the pelvis: inclusion of muscular and ligamentous boundary conditions, Med. Eng. Phys. 29 (7) (2007) 739–748, https://doi.org/10.1016/j.medengphy.2006.08.010.

[48] W. Kou, Y. Liang, Z. Wang, et al., An integrated method of biomechanics modeling for pelvic bone and surrounding soft tissues, Bioengineering 10 (6) (2023) 736, https://doi.org/10.3390/bioengineering10060736.

[49] Loay A. Salman, A. Al-Ani, M.F.A. Radi, et al., Open versus closed intramedullary nailing of femur shaft fractures in adults: a systematic review and meta-analysis, Int. Orthop. 47 (12) (2023) 3031–3041.

[50] Z. Xu, X. Zhang, Y. Wang, et al., Comparison of Bone-setting Robots and Conventional Reduction in the Treatment of Intertrochanteric Fracture: a Retrospective Study, Orthop. Surg. 16 (2) (2024) 312–319.

[51] A. Segato, F. Calimeri, I. Testa, et al., A hybrid inductive learning-based and deductive reasoning-based 3-D path planning method in complex environments, Auton. Robots 46 (5) (2022) 645–666.

[52] M. Shah, N. Patel, FNPG-NH: a Reinforcement Learning Framework for Flexible Needle Path Generation With Nonholonomic Constraints, IEEe Robot. Autom. Lett. (2023).

[53] H. Tian, C. Song, C. Wang, et al., Sampling-based planning for retrieving near-cylindrical objects in cluttered scenes using hierarchical graphs, IEEE Trans. Robot. 39 (1) (2022) 165–182.